Efficient surface passivation of germanium nanostructures with 1% reflectance

OPEN ACCESS
IOP Publishing
Nanotechnology

Nanotechnology **34** (2023) 355201 (9pp)
https://doi.org/10.1088/1361-6528/acd25b

Efficient surface passivation of germanium nanostructures with 1% reflectance

Tsun Hang Fung[1,*], Joonas Isometsä[1], Juha-Pekka Lehtiö[2], Toni P Pasanen[1], Hanchen Liu[1], Oskari Leiviskä[1], Pekka Laukkanen[2], Hele Savin[1] and Ville Vähänissi[1]

[1] Department of Electronics and Nanoengineering, Aalto University, FI-02150 Espoo, Finland
[2] Department of Physics and Astronomy, University of Turku, FI-20014 Turku, Finland

E-mail: john.h.fung@aalto.fi

Received 22 March 2023, revised 24 April 2023
Accepted for publication 3 May 2023
Published 13 June 2023

Abstract

Germanium (Ge) is a vital element for applications that operate in near-infrared wavelengths. Recent progress in developing nanostructured Ge surfaces has resulted in >99% absorption in a wide wavelength range (300–1700 nm), promising unprecedented performance for optoelectronic devices. However, excellent optics alone is not enough for most of the devices (e.g. PIN photodiodes and solar cells) but efficient surface passivation is also essential. In this work, we tackle this challenge by applying extensive surface and interface characterization including transmission electron microscopy and x-ray photoelectron spectroscopy, which reveals the limiting factors for surface recombination velocity (SRV) of the nanostructures. With the help of the obtained results, we develop a surface passivation scheme consisting of atomic-layer-deposited aluminum oxide and sequential chemical treatment. We achieve SRV as low as 30 cm s^{-1} combined with ~1% reflectance all the way from ultraviolet to NIR. Finally, we discuss the impact of the achieved results on the performance of Ge-based optoelectronic applications, such as photodetectors and thermophotovoltaic cells.

Keywords: nanotexturing, surface passivation, photodetector, germanium, ICP-RIE, ALD, chemical residuals

(Some figures may appear in colour only in the online journal)

Introduction

Germanium (Ge) is a promising candidate in several technological areas, due to the attractiveness governed by its intrinsic properties [1–7]. In particular, Ge has a relatively small bandgap, making it an ideal candidate for optoelectronic devices operating in the near-infrared (NIR) region, such as photodiodes and thermophotovoltaic (TPV) devices [5–9]. Nevertheless, planar Ge surfaces suffer from high reflectance (~40% at 1550 nm) resulting in significant optical loss limiting the performance of Ge-based optoelectronic devices. To address the optical losses, anti-reflective coatings have been the mainstream technology in the state-of-the-art Ge devices, although the coating can only be optimized for a limited wavelength range. In recent years, significant research efforts have been devoted to further reduce the surface reflectance of Ge. One approach is to use dielectric metasurfaces that aim to control the local polarizations, phases, and field amplitudes of light, resulting in enhanced absorption especially in thin layers [10, 11]. Another alternative is to form a graded-index medium between air and the Ge substrate by nanostructures etched on Ge surface (i.e. black Ge) either via metal assisted chemical etching [7, 8, 12, 13] or plasma etching (i.e. reactive-ion etching (RIE) or inductively-coupled plasma etching (ICP-RIE). Out of all these methods, ICP-RIE has been the most promising achieving as low as sub-1% surface reflectance all the way from ultraviolet up to NIR (~1700 nm) [9, 14, 15].

* Author to whom any correspondence should be addressed.

The excellent optics provided by the nanostructures has already been utilized in some devices such as metal-semiconductor-metal and Schottky photodiodes [7, 9]. However, most optoelectronic devices (such as PIN-photodiodes and solar cells) are minority carrier based, thus, besides optical properties, excellent electrical properties such as minority carrier lifetime are also of vital importance. In this regard, surface passivation—a process that aims to minimize surface recombination—plays a critical role for nanostructured surfaces. Quite surprisingly, while successful surface passivation of nanostructured silicon has been reported in literature [16–19], similar studies have not been reported for Ge. In other words, there are only some interface defect density results for microscale structures [8] but no direct data on surface passivation of nanostructured Ge. However, for planar Ge surfaces, there are extensive studies. A natural material choice for the surface passivation would be germanium oxides, but they are known to be highly unstable and water-soluble preventing their use in practical applications [20]. Recently, aluminum oxide (Al_2O_3) deposited via atomic layer deposition (ALD) has become the forefront in surface passivation [21–24]. It has been demonstrated that ALD Al_2O_3 forms negative fixed charge at the Al_2O_3–Ge interface resulting in excellent surface passivation through field-effect [21, 24]. Prior to ALD either HCl or HF alone is often used instead of RCA cleaning, which has been shown to be too vigorous for Ge [25–28]. In addition to cleaning the surface, another purpose of this treatment is to remove unstable native germanium oxides that easily form on the surface when exposed to air [29–31]. These results serve as a good starting point for nanoscale structures as well due to the conformality of ALD. However, this is not enough as the nanostructures bring several additional challenges. Firstly, the surface area is significantly enhanced as a consequence of needle-like nanostructures inherently increasing the number of dangling bonds at the surface. Secondly, ion-bombardment as a part of dry etching raises the concern of creating crystallographic damage on the surface, which could result in a so-called 'dead-layer' with extensive amount of recombination sites near the surface [16, 32–34]. Thirdly, the use of processing gases during dry etching results in chemical residuals on the nanotextured surface [35]. To fully utilize the potential of black Ge in devices without tradeoffs in electrical and optical properties, these challenges need to be addressed.

In this work, we develop an efficient surface passivation scheme for black Ge based on ALD Al_2O_3. More specifically, we investigate and address the three aspects that are concerned when integrating black Ge into optoelectronic devices: (1) surface area enhancement, (2) crystallographic damage caused by ion-bombardment and (3) chemical residuals remaining on nanotextured surfaces. The corresponding electrical properties are evaluated using quasi-steady state photoconductance decay. The crystallinity of the Ge after subjecting to ICP-RIE is investigated by transmission electron microscopy (TEM) and the chemical residuals on the Ge surface at different stages are monitored by x-ray photoelectron spectroscopy (XPS). Finally, the impact of the obtained results on optoelectronic devices is discussed.

Determining limiting factors for surface passivation

Increased surface area

Figure 1 shows the surface morphology for the two sets of nanotexture used in this study, fabricated by using ICP-RIE with an ICP power of 1000 W. First, a 700 nm deep nanotexture (figure 1(a)) was formed by using capacitively-coupled plasma (CCP) power of 4 W, which results in black Ge with a broadband surface reflectance of less than 1% [15]. The inset shows an optical image of the full 4 inch wafer to demonstrate the black appearance by naked eye. Second, a shallow nanotexture of ∼200 nm height (figure 1(b)) was formed by using CCP power of 2 W, which results in completely different morphology i.e. only moderately increases the surface area compared to a planar surface. These two morphologies allow us to study the impact of the increased surface area on the passivation.

To determine the starting level of surface passivation of the Ge nanostructures, for the first experiment we chose the passivation scheme that has provided the best performance on planar Ge [36]. After subjecting to a HCl cleaning for 5 min, we deposited a 20 nm thick Al_2O_3 conformally on the nanotexture and activated the surface passivation by performing a 400 °C post-deposition anneal. As expected, for a planar germanium reference sample, ALD Al_2O_3 provided excellent surface passivation resulting in a lifetime above 1 ms, as shown in figure 2 [21, 24]. For the deep nanostructures, the same passivation scheme leads to substantially lower lifetime around 200 μs (blue markers). Surprisingly, for shallow nanostructures (green markers) there is no significant improvement despite the drastic difference between the surface morphology shown by the SEM images. Therefore, it is clear that surface area enhancement, due to the formation of nanotextures, is not the primary factor limiting the lifetime for the nanotextured samples.

Crystallographic damage

There has been a pervasive concern on surface damage induced by RIE [7, 8], hence, to elucidate the role of ion-bombardment on the poor effective lifetime measured on nanotextured samples, the crystallinity of the nanotextured Ge was examined in detail at the Al_2O_3–Ge interface by using TEM. As shown in figure 3, Ge lattice at the proximity of the Al_2O_3–Ge interface remains crystalline as no amorphous-like structure is observed, akin to what has been demonstrated on black silicon fabricated by the same method [17]. Consequently, the poor effective lifetime shown above is not caused by ion-bombardment during the etching process. Since no crystallographic damage was observed for the deep nanotexture, the same conclusion can be drawn from the shallow structures, as the degree of ion-bombardment correlates to the magnitude of CCP power, which was reduced from 4 to 2 W [16]. In summary, this result clearly demonstrates that it is possible to fabricate Ge nanotexture by ICP-RIE that is free of crystallographic damage.

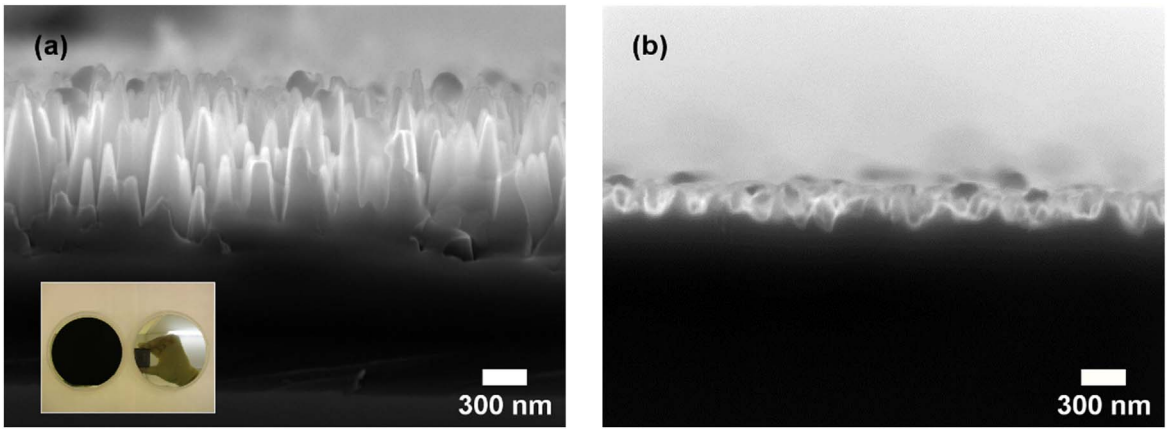

Figure 1. Cross-sectional SEM images: (a) a deep nanotexture fabricated by using 4 W capacitively-coupled plasma power (inset showing an optical image of the corresponding 4 inch Ge wafer) and (b) a shallow nanotexture fabricated by using 2 W capacitively-coupled plasma power.

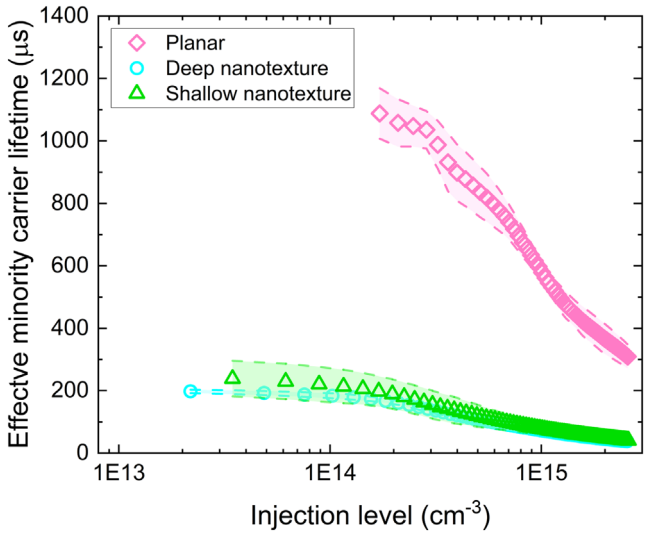

Figure 2. Injection-dependent effective minority carrier lifetime of HCl-cleaned ALD Al_2O_3 passivated Ge samples with a planar surface (pink rhombus), a deep nanotexture (blue circule) and a shallow nanotexture (green triangle).

Chemical residues

Since neither the enhanced surface area nor the crystal damage explains the poor lifetime of the black Ge, next we studied whether some chemical residuals formed during dry etching could be the root cause. Figures 4(a) and (b) shows the XPS spectra of the S 2p and F 1s bonding states measured at the surface of the nanotexture directly after the ICP-RIE process. A significant amount of sulfur and fluoride elements were detected on both deep and shallow nanotextures. (Note that there is a much higher amount of residuals detected on the shallow nanotexture, which could be due to the use of higher process gas flows and a lower CCP power during the ICP-RIE etching process.) As shown in figure 4(c), after 5 min of HCl cleaning, the sulfur elements with a higher binding energy were removed, while the ones with a lower binding energy remain on the surface. On the other hand, all the fluoride elements were removed for both sets of nanotexture (figure 4(d)). The removed elements are likely associated with oxide compounds, as HCl has shown to be efficient in removing oxide from germanium surface [31]. To conclude, HCl is not able to remove all the chemical residues and most likely the remaining sulfur-related residuals cause the poor surface passivation. We speculate the following mechanisms for this: (i) they could act as recombination-sites at the Al_2O_3–Ge interface, which increases the interface defect density, (ii) they could also hinder the subsequent activation of the Al_2O_3 layer during the post-deposition annealing, which reduces the fixed charge density at the interface. Nevertheless, the exact mechanism is difficult to identify, due to the ambiguous analysis of *C–V* measurements on nanotextured surface.

Keys to excellent electrical and optical properties

Removal of chemical residues

As the XPS results demonstrated above, HCl alone leaves some sulfur-related residuals on the surface of Ge nanotexture. In order to remove them prior to thin film deposition, we applied a chemical cleaning process composed of H_2O_2 and HCl sequentially. Since germanium dioxide is water soluble, the Ge atoms at the surface, when subjecting to H_2O_2 solution, are readily oxidized and then dissolved in the solution [37]. Therefore, we speculate that the sulfur-related residuals could be removed along with the Ge atoms by performing an additional H_2O_2 dip. The subsequent HCl dip, on the other hand, efficiently removes any sub-oxide remaining on the Ge nanotexture and results in Cl-termination of the surface, which protects the Ge nanotexture from being oxidized in the air prior to ALD passivation [31, 37]. As shown in figure 5, according to our hypothesis, the sulfur-related residuals detected on the nanotexture after HCl cleaning alone were found to be removed completely after an addition of a 10 s H_2O_2 dip. As a result, the level of surface contamination for the Ge nanotexture after 10 s of H_2O_2 cleaning should be similar to the planar Ge surface without any ICP-RIE etching.

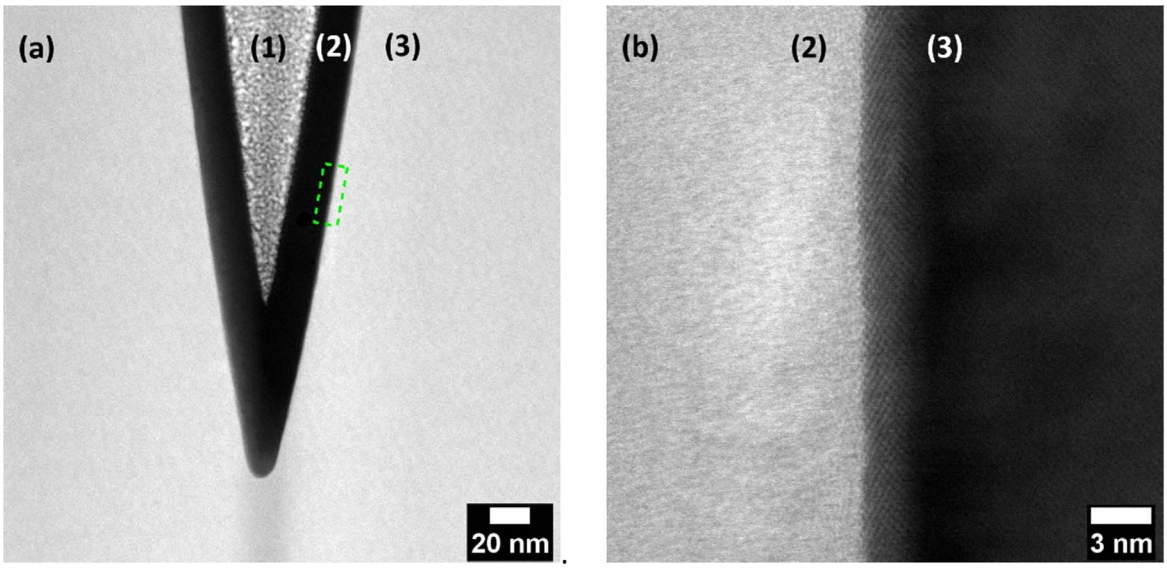

Figure 3. (a) A dark field transmission electron microscope image of a deep nanotexture coated with a 20 nm Al_2O_3 layer at 500 000 times magnification. Sub-labels (1), (2) and (3) indicate a region of sputtered platinium, Al_2O_3 layer and Ge, respectively. Green dashed-box highlights the area where the image with the higher magnification was taken. (b) A bright field transmission electron microscope image at 5 million times magnification. Sub-labels (2) and (3) indicate a region of Al_2O_3 layer and Ge, respectively.

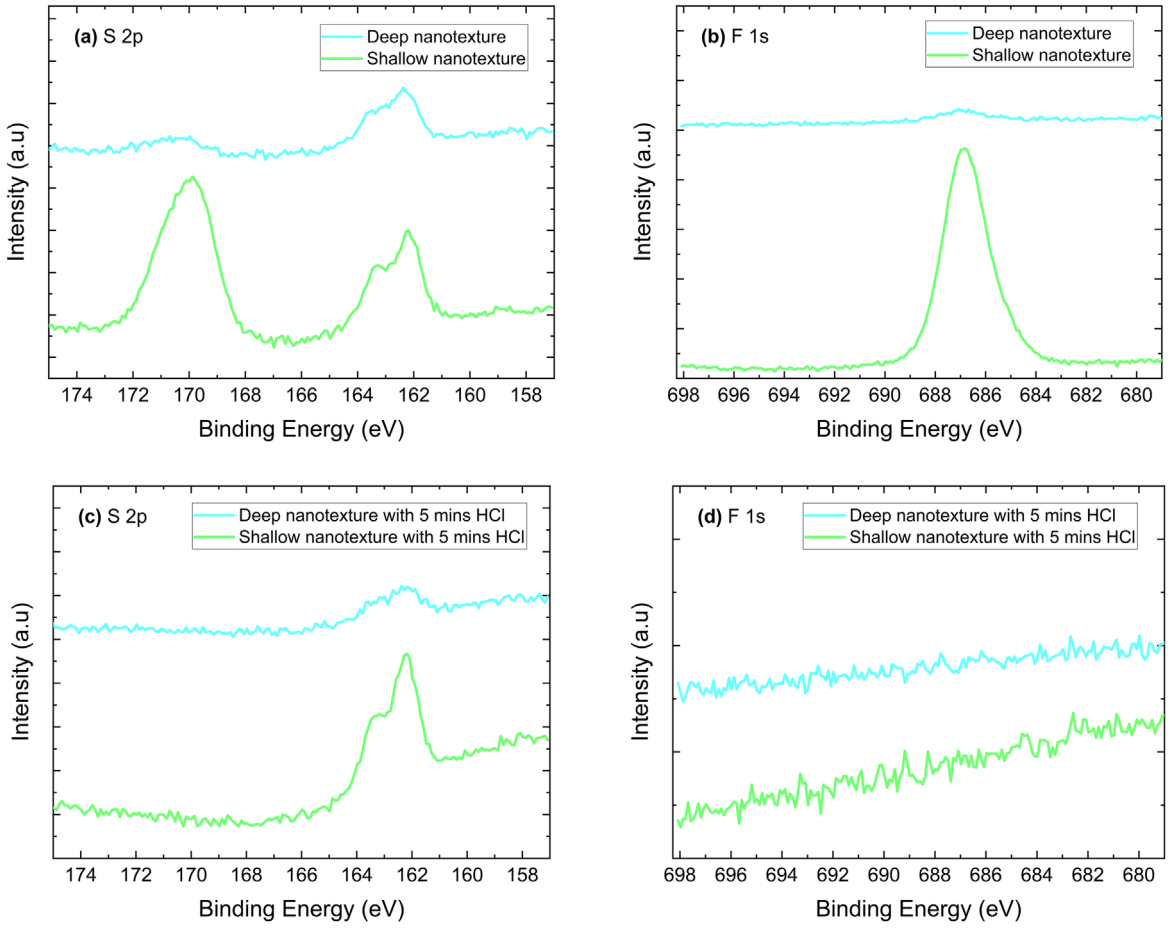

Figure 4. X-ray photoelectron spectroscopy measurement of a deep nanotexture (cyan) and a shallow nanotexture (green): (a) S 2p level prior to a HCl cleaning, (b) F 1s level prior to a HCl cleaning, (c) S 2p level after 5 min of HCl cleaning and (d) F 1s level after 5 min of HCl cleaning.

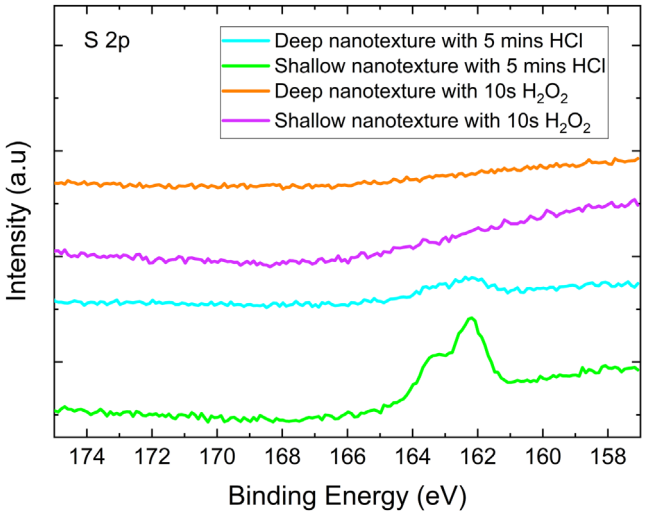

Figure 5. X-ray photoelectron spectroscopy measurement of S 2p level for a deep nanotexture and a shallow nanotexture with and without additional H_2O_2 dip.

Figure 6(a) shows what is the minority carrier lifetime after successful chemical residue removal. The addition of a 10 s cleaning in H_2O_2 solution increases the effective minority carrier lifetime of the deep nanotexture by two-folds, reaching over 400 μs in the low-injection region. As the combination of oxidation and dissolution of Ge atoms during the H_2O_2 dip likely also modulates the nanotexture morphology, the impact of this cleaning treatment on the surface reflectance and morphology needs to be investigated. The surface reflectance of the deep nanotexture after 10 s H_2O_2 cleaning remains sub-1% (figure 6(b)), as the features are largely intact, with only some rounding observed at the tip of the nanotexture. As another significant observation, it was found that the deep nanotexture with an addition of 10 s H_2O_2 treatment (orange star) resulted in a noticeably higher lifetime (400 μs versus 240 μs) when compared to the shallow nanotexture treated with HCl alone (green triangle) despite having a substantially higher surface area and a lower surface reflectance. Since the attribute of crystal damage has been excluded by the TEM image shown above, it is likely that the difference in surface contamination prior to ALD deposition, due to the addition of H_2O_2 cleaning, contributes to the difference in lifetime measured for both sets of nanotextures. Removing all the chemical residuals is, therefore, demonstrated to be a crucial factor in achieving good surface passivation for Ge nanotexture created by ICP-RIE process.

In the case of shallow nanostructures the addition of H_2O_2 cleaning was found to affect significantly the morphology by removing most of the features resulting in a planar-like surface. Consequently, the lifetime was improved from sub-300 μs to over 900 μs. The obtained value is clearly higher than in the deep nanostructure counterpart. This difference is likely due to the difference in the surface area. Consequently, it is suggested that the lifetime of the deep nanotexture after 10 s of H_2O_2 cleaning is limited by the significantly larger surface area when compared to the planar-like surface.

Finding balance between reflectance and surface recombination

From the perspective of a device, it is crucial to consider both electrical and optical properties of black Ge. The successful removal of chemical residuals on the Ge nanotexture resulted in significant improvement in lifetime. However, the lifetime was still found out to be much lower than the corresponding planar sample. This means that after chemical residue removal the lifetime of black Ge is limited by the surface area —a factor which also contri-ance of black Ge. Hence, there is a clear need for a tradeoff between the reflectance and the lifetime. We aimed to minimize this tradeoff by modulating the surface morphology with the application of an extended H_2O_2 treatment, i.e. by reducing the surface area as much as possible without meaningfully increasing the surface reflectance. Figure 7 shows the impact of an extended H_2O_2 treatment on the morphology of a deep nanotexture. As mentioned earlier, a 700 nm deep nanotexture is formed on Ge surface by ICP-RIE, whereas some rounding at the tip (due to the combination of oxidation and dissolution of Ge atoms) is observed after subjecting to 10 s H_2O_2 treatment. As the duration of H_2O_2 treatment increases, the modulation of the surface morphology becomes increasingly significant, leading to pyramidal structures with a $\sim$54° facet angle after 120 s. Interestingly, the facet angle for the nanotexture observed in figure 7(d) coincides with the angle difference between the {100} and {111} for a diamond cubic crystal structure, which is commonly observed in silicon with alkaline chemical texturing [38]. It has also been observed in germanium with inverted pyramidal surface fabricated by the combination of lithography and metal-assisted chemical etching [7, 39].

In order to analyze the tradeoff between electrical and optical properties after different H_2O_2 cleaning durations, figure 8 summarizes both the surface recombination velocity (SRV) and the front surface reflectance at 1550 nm for all the samples. The deep nanotexture reduces the surface reflectance compared to the planar surface from over 35% to sub-1%. The surface reflectance of the deep nanotexture does not meaningfully increase by the H_2O_2 treatment until 30 s is reached, beyond which it increases significantly to over 20% after 120 s. This significant increase in surface reflectance is expected, as the surface morphology is drastically modified after 120 s of H_2O_2 treatment. On the other hand, the formation of the deep nanotexture substantially increases the SRV as compared to the planar surface from 6 cm s^{-1} to over 100 cm s^{-1}. After 10 s H_2O_2 treatment, the SRV reduces by half, reaching 40 cm s^{-1}. Further increase in duration leads to further reduction in SRV, with 30 cm s^{-1} and 10 cm s^{-1} measured after 30 s and 120 s, respectively. Consequently, a very good combination of both optical and electrical quality is reached with 30 s H_2O_2 cleaning resulting in $\sim$1% reflectance and SRV of $\sim$30 cm s^{-1}. The exact optimal etching time depends on the desired properties of the device.

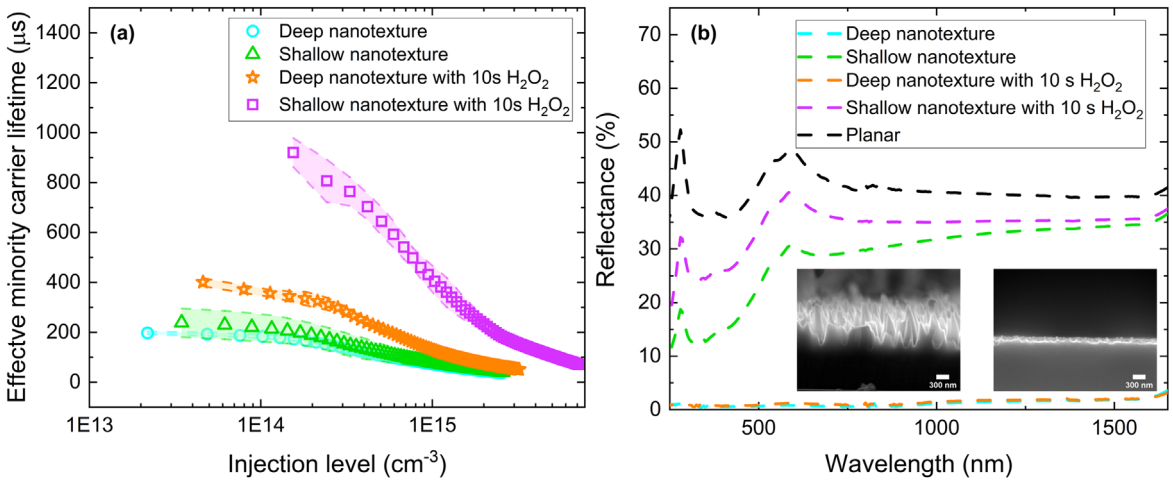

Figure 6. (a) Injection-dependent effective minority carrier lifetime and (b) wavelength-dependent front surface reflectance of Ge samples with a deep nanotexture (cyan circle and dashed-line), a shallow nanotexture (green triangle and dashed-line), a deep nanotexture with 10 s H_2O_2 cleaning (orange star and dashed-line), a shallow nanotexture with 10 s H_2O_2 cleaning (purple square and dashed-line) and a planar surface (black dashed-line). Embedded SEM images: a deep nanotexture (left) and a shallow nanotexture (right) after 10 s of H_2O_2 cleaning.

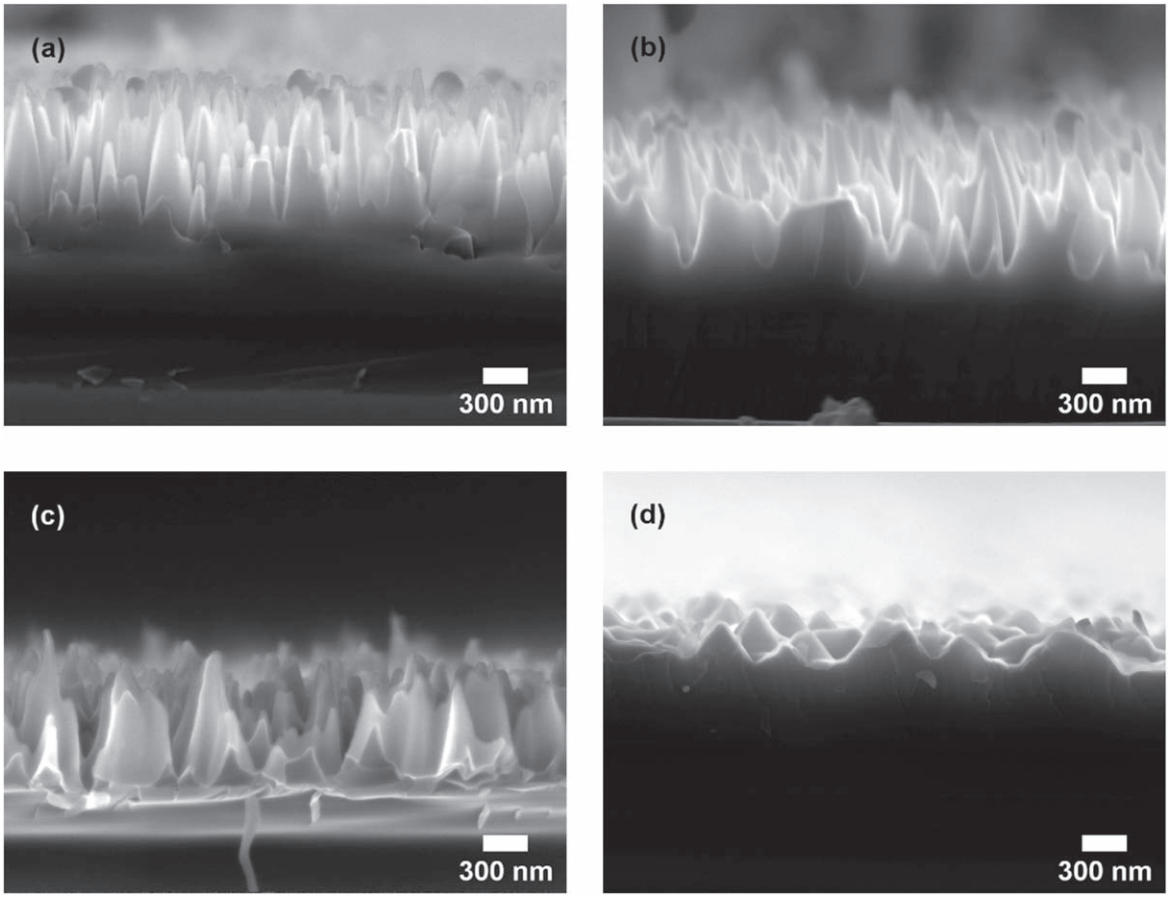

Figure 7. Cross-sectional SEM images of a deep nanotexture with various duration of H_2O_2 cleaning: (a) as-etched, (b) 10 s, (c) 30 s and (d) 2 min.

Discussion

The above results demonstrate successful electrical passivation of black Ge nanostructures without increasing the surface reflectance. This was achieved by combining H_2O_2 cleaning to remove chemical residuals originating from ICP-RIE with ALD Al_2O_3 surface passivation, which is industrially feasible and should be relatively straightforward to integrate into device fabrication. The achieved excellent opto-electrical properties have tremendous potential in opening new opportunities for further advancing the performance of Ge-based

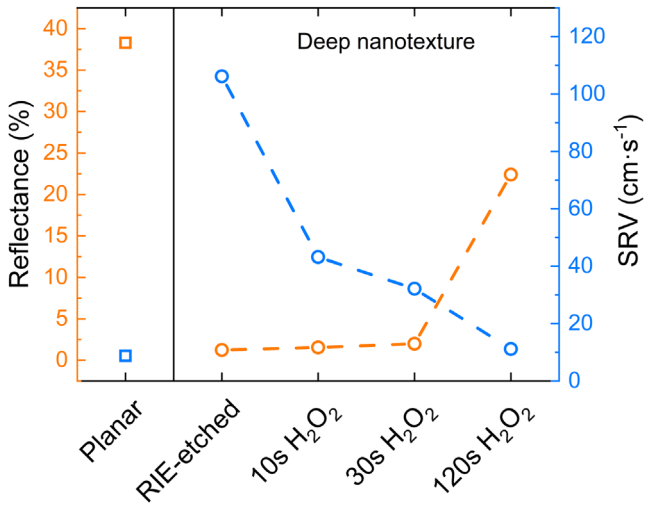

Figure 8. Front surface reflectance at 1550 nm (orange) and surface recombination velocity at injection level of 2×10^{14} cm^{-3} (blue) for the deep nanotexture after various H_2O_2 cleaning times (circles). Corresponding values for the planar surface (squares) are given as a reference.

optoelectronic devices and/or fully utilizing the already existing advantages (e.g. quantum confinement, photo gating, negative differential resistance) demonstrated by nanostructured Ge devices [40–43]. For instance, in NIR photodiodes the method should enable much higher photoresponsivity around the two main wavelengths used in fiber optics (1300 and 1550 nm). In addition to NIR region, the results show a high promise also at lower wavelengths all the way to UV (300 nm). Recently, in silicon photodiodes, carrier multiplication at short wavelengths has been successfully harnessed for extremely high EQE [36]. Since Ge has much lower bandgap (0.66 eV at 300 K), harnessing carrier multiplication should be possible in much wider wavelength range possibly leading to above unity EQE up to ~600 nm.

Another potential application where black Ge with low surface recombination should bring significant benefit is a TPV cell. It could be directly incorporated into the interdigitated-back-contact (IBC) cell architecture—a TPV cell design with higher theoretical conversion efficiency (up to 25%) [44] than conventional state-of-the-art Ge-based TPV devices (16.5%) [45, 46]—creating an avenue for achieving near-unity EQE, akin to what has been demonstrated in black Si IBC cell for different wavelength spectrum, whereas the EQE of current standalone Ge TPV devices fall between 60% and 80% [6, 47, 48].

Conclusions

This paper demonstrates, for the first time, efficient surface passivation of nanostructured Ge surfaces fabricated by ICP-RIE. First, we defined the limiting factors preventing effective surface passivation by conventional ALD Al_2O_3. While TEM analysis ruled out the presence of crystallographic damage, XPS confirmed that the root cause lies in sulfur-related chemical residues that were remaining on the surface after HCl cleaning. By adding a short H_2O_2 dip, we were able to remove all the chemical residuals on the nanostructured surfaces, resulting in a two-fold increase in effective lifetime. After chemical residue removal, the next factor limiting the lifetime was found to be the increased surface area. To find a balance between electrical and optical properties, the surface area was reduced by extending the duration of the H_2O_2 dip. Consequently, the SRV of nanostructured Ge further reduced from ~100 to ~30 cm s^{-1} without impact on the front surface reflectance. These results enable nanostructured Ge to be a key building-block for further advancing the performance of Ge-based optoelectronics devices, such as photodetectors and TPV cells.

Experimental section

Sample fabrication. A batch of 187 μm thick, double-sided polished 4 inch *n*-type {100} Czochralski (CZ) germanium wafers with a 18–25 Ω cm base resistivity were used in these experiments. The Ge nanotexture was fabricated by using cryogenic inductively-coupled plasma reactive-ion etching (ICP-RIE, Plasmalab System 100, Oxford Instruments) at −120 °C for 15 min using SF_6 and O_2 as the processing gases. Whilst the power of the ICP source was kept at 1000 W for both processes, a CCP power of 4 W and 2 W was used to form a deep and a shallow nanotexture, respectively. During both deep and shallow nanotexture etching, the DC bias was measured to be 0 V. For the deep nanotexture sample, the gas flows for SF_6 and O_2 were 17 and 22.8 sccm, respectively. For the shallow nanotexture sample, due to the significant reduction in etch-rate, the gas flows were increased to 21.5 and 28.4 sccm for SF_6 and O_2, respectively. The chamber pressure was kept at 10 mTorr for all samples.

Two chemical cleaning processes were investigated in this study: (1) a HCl dip and (2) a sequential chemical treatment. In the HCl cleaning process, the samples were cleaned by dipping them into HCl (31.6% v/v) for 5 min without a subsequent DIW rinsing (to avoid oxidation) prior to ALD deposition. For the sequential cleaning process, the samples were cleaned by dipping them into different chemical solutions in the following order: (1) 3% v/v of H_2O_2 for 2 min, (2) 31.6% v/v of HCl for 5 min, (3) 3% v/v of H_2O_2 for varied duration and (4) 31.6% v/v of HCl for 5 min By varying the duration of step (3), the amount of Ge atoms being removed by this process was modulated. DIW rinsing was applied between each step, but not after step (4) was completed. An Al_2O_3 layer (n = 1.65 at 633 nm, thickness = 22.5 nm) was subsequently deposited by thermal ALD at 200 °C. The number of cycles was 200 and H_2O and TMA were used as precursors. Finally, the samples were annealed at 400 °C for 30 min under nitrogen ambient to activate the passivation.

Sample characterization. The injection-dependent effective minority carrier lifetime was measured by using QSS-μPCD technique in a Semilab PV2000A characterization tool. The measured lifetime was then converted to SRV, a useful metric in examining the quality of surface passivation, by the

following equation [49]

$$\frac{1}{\tau_{\text{eff}}(\Delta n)} = \frac{1}{\tau_b(\Delta n)} + \frac{1}{\tau_s(\Delta n)} = \frac{1}{\tau_b(\Delta n)} + \frac{2S_{\text{eff}}(\Delta n)}{W} \rightarrow S_{\text{eff,max}}(\Delta n) = \frac{W}{2\tau_{\text{eff}}(\Delta n)}, \quad (1)$$

where W (cm) and Δn (cm^{-3}) represent the wafer thickness and excess carrier density, respectively. The above calculation assumes that the bulk recombination is negligible, and hence the calculated $S_{\text{eff,max}}$ represents the maximum value. For single-sided RIE-etched sample, the SRV of the textured surface was evaluated by the following equation

$$S_{\text{eff,textured}}(\Delta n) = \frac{W}{\tau_{\text{eff}}(\Delta n)} - S_{\text{eff,planar}}(\Delta n), \quad (2)$$

where $S_{\text{eff,planar}}$ represents the SRV of the planar surface extracted from a planar reference sample using equation (1). The front surface reflectance between 300 nm and 1700 nm was measured by using an integrating sphere in Agilent Cary 5000 UV–vis-NIR spectrophotometer. The surface morphology of the nanotextures was inspected by cross-sectional scanning electron microscopy using Zeiss Supra 40. The crystallinity of the germanium at the Al_2O_3–Ge interface was inspected by TEM using JEOL JEM-2200FS. The TEM lamella was prepared by lift-out focused-ion beam (JEOL JIB-4700F) with sputtered platinum acting as a protective layer. The surface chemistry of the nanotexture prior to ALD was analyzed by XPS using Thermo Scientific (tm) Nexsa instrument with monochromated Al $K\alpha$ source.

Acknowledgments

The authors thank the ATTRACT project funded by the European Commission (EC), under Agreement No. 777222 and No. 101004462. The authors also thank Business Finland (Project No. RaPtor 687/31/2019) and the Academy of Finland (Project Nos. 328482, 331313, and 338974) for financial support. The work was partially funded by Tandem Industry Academia funding from the Finnish Research Impact Foundation. The work has also received funding from the EMPIR program co-financed by the Participating States and from the European Union's Horizon 2020 research and innovation program (project 19ENG05 NanoWires) The work is also related to the Flagship on Photonics Research and Innovation 'PREIN' funded by the Academy of Finland. The authors acknowledge the provision of facilities and technical support by the Micronova Nanofabrication Centre in Espoo, Finland, within the OtaNano research infrastructure at Aalto University.

Data availability statement

All data that support the findings of this study are included within the article (and any supplementary files).

ORCID iDs

Tsun Hang Fung https://orcid.org/0000-0002-5768-9166
Joonas Isometsä https://orcid.org/0000-0003-2339-4586
Juha-Pekka Lehtiö https://orcid.org/0000-0002-4762-8554
Toni P Pasanen https://orcid.org/0000-0003-1218-7303
Hanchen Liu https://orcid.org/0000-0002-8404-4902
Oskari Leiviskä https://orcid.org/0009-0009-8897-8348
Pekka Laukkanen https://orcid.org/0000-0003-4220-985X
Hele Savin https://orcid.org/0000-0003-3946-7727
Ville Vähänissi https://orcid.org/0000-0002-2681-5609

References

[1] Gupta S, Magyari-Köpe B, Nishi Y and Saraswat K C 2013 Achieving direct band gap in germanium through integration of Sn alloying and external strain *J. Appl. Phys.* **113** 073707
[2] Fadaly E M T, Dijkstra A, Suckert J R, Ziss D, van Tilburg M A J, Mao C, Ren Y, van Lange V T, Korzun K, Kölling S, Verheijen M A, Busse D, Rödl C, Furthmüller J, Bechstedt F, Stangl J, Finley J J, Botti S, Haverkort J E M and Bakkers E P A M 2020 Direct-bandgap emission from hexagonal Ge and SiGe alloys *Nature* **580** 205–9
[3] Sun X, Liu J, Kimerling L C and Michel J 2010 Toward a germanium laser for integrated silicon photonics *IEEE J. Sel. Top. Quantum Electron.* **16** 124–31
[4] Ye P, Ernst T and Khare V M 2019 The last silicon transistor *IEEE Spectr.* **58** 31–5
[5] van der Heide J, Posthuma N E, Flamand G, Geens W and Poortmans J 2009 Cost-efficient thermophotovoltaic cells based on germanium substrates *Sol. Energy Mater. Sol. Cells* **93** 1810–6
[6] Alcañiz A, López G, Martín I, Jiménez A, Datas A, Calle E, Ros E, Gerling L G, Voz C, del Cañizo C and Alcubilla R 2019 Germanium photovoltaic cells with MoOx hole-selective contacts *Sol. Energy* **181** 357–60
[7] Kim M *et al* 2018 Enhanced performance of Ge photodiodes via monolithic antireflection texturing and α-Ge self-passivation by inverse metal-assisted chemical etching *ACS Nano* **12** 6748–55
[8] Shin S H, Liao Y, Son B, Zhao Z J, Jeong J H, Tan C S and Kim M 2021 A highly ordered and damage-free Ge inverted pyramid array structure for broadband antireflection in the mid-infrared *J. Mater. Chem.* C **9** 9884–91
[9] An S, Liao Y, Shin S and Kim M 2021 Black Germanium photodetector exceeds external quantum efficiency of 160% *Adv. Mater. Technol.* **2100912** 1–7
[10] Tian J, Li Q, Belov P A, Sinha R K, Qian W and Qiu M 2020 High- Q All-Dielectric metasurface: super and suppressed optical absorption *ACS Photonics* **7** 1436–43
[11] Yu J, Ma B, Ouyang A, Ghosh P, Luo H, Pattanayak A, Kaur S, Qiu M, Belov P and Li Q 2021 Dielectric super-absorbing metasurfaces via PT symmetry breaking *Optica* **8** 1290
[12] Chen K, Isometsä J, Pasanen T P, Vähänissi V and Savin H 2020 Efficient photon capture on germanium surfaces using industrially feasible nanostructure formation *Nanotechnology* **32** 035301
[13] Zhang Y Y, Shin S H, Kang H J, Jeon S, Hwang S H, Zhou W, Jeong J H, Li X and Kim M 2021 Anti-reflective porous Ge by open-circuit and lithography-free metal-assisted chemical etching *Appl. Surf. Sci.* **546** 149083
[14] Steglich M, Käsebier T, Kley E B and Tünnermann A 2016 Black Germanium fabricated by reactive ion etching *Appl. Phys. A Mater. Sci. Process.* **122** 1–5

[15] Pasanen T P, Isometsä J, Garin M, Chen K, Vähänissi V and Savin H 2020 Nanostructured Germanium with >99% absorption at 300–1600 nm wavelengths *Adv. Opt. Mater.* **8** 1–5

[16] Plakhotnyuk M M, Gaudig M, Davidsen R S, Lindhard J M, Hirsch J, Lausch D, Schmidt M S, Stamate E and Hansen O 2017 Low surface damage dry etched black silicon *J. Appl. Phys.* **122** 143101

[17] Von Gastrow G, Alcubilla R, Ortega P, Yli-Koski M, Conesa-Boj S, Fontcuberta I, Morral A and Savin H 2015 Analysis of the Atomic Layer Deposited Al2O3 field-effect passivation in black silicon *Sol. Energy Mater. Sol. Cells* **142** 29–33

[18] Iandolo B, Sánchez Nery A P, Davidsen R S and Hansen O 2019 Black silicon with ultra-low surface recombination velocity fabricated by inductively coupled power plasma *Phys. Status Solidi - Rapid Res. Lett.* **13** 1–5

[19] Repo P, Haarahiltunen A, Sainiemi L, Yli-Koski M, Talvitie H, Schubert M C and Savin H 2013 Effective passivation of black silicon surfaces by atomic layer deposition *IEEE J. Photovoltaics* **3** 90–4

[20] Xie Q, Deng S, Schaekers M, Lin D, Caymax M, Delabie A, Qu X P, Jiang Y L, Deduytsche D and Detavernier C 2012 Germanium surface passivation and atomic layer deposition of high-k dielectrics—a tutorial review on Ge-based MOS capacitors *Semicond. Sci. Technol.* **27** 074012

[21] Berghuis W J H, Melskens J, Macco B, Theeuwes R J, Verheijen M A and Kessels W M M 2021 Surface passivation of germanium by atomic layer deposited Al_2O_3 nanolayers *J. Mater. Res.* **36** 571–81

[22] Berghuis W J H, Melskens J, Macco B, Theeuwes R J, Black L E, Verheijen M A and Kessels W M M 2021 Excellent surface passivation of germanium by a-Si:H/Al_2O_3 stacks *J. Appl. Phys.* **130** 135303

[23] Martín I, López G, Garín M, Voz C, Ortega P and Puigdollers J 2022 Effect of the thickness of amorphous silicon carbide interlayer on the passivation of c-Ge surface by aluminium oxide films *Surfaces and Interfaces* **31** 102070

[24] Isometsä J, Fung T H, Pasanen T P, Liu H, Yli-Koski M, Vähänissi V and Savin H 2021 Achieving surface recombination velocity below 10 cm/s in n-type germanium using ALD Al2O3 *APL Mater.* **9** 3–10

[25] Sioncke S, Brunco D P, Meuris M, Uwamahoro O, Van Steenbergen J, Vrancken E and Heyns M M 2009 Etch rate study of germanium, GaAs, and InGaAs: a challenge in semiconductor processing *Solid State Phenom.* **145–146** 203–6

[26] Brunco D P *et al* 2008 Germanium MOSFET devices: advances in materials understanding, process development, and electrical performance *J. Electrochem. Soc.* **155** H552

[27] Sioncke S, Brunco D P, Meuris M, Uwamahoro O, Van Steenbergen J, Vrancken E and Heyns M M 2019 Etch rates of Ge, GaAs and InGaAs in acids, bases and peroxide based mixtures *ECS Trans.* **16** 451–60

[28] Abrenica G H A, Fingerle M, Lebedev M V, Arnauts S, Mayer T, Holsteyns F, de Gendt S and van Dorp D H 2020 Wet chemical processing of Ge in Acidic H 2 O 2 solution: nanoscale etching and surface chemistry *ECS J. Solid State Sci. Technol.* **9** 084002

[29] Zhang S, Hemesath E R, Perea D E, Wijaya E, Lensch-Falk J L and Lauhon L J 2009 Relative influence of surface states and bulk impurities on the electrical properties of ge nanowires *Nano Lett.* **9** 3268–74

[30] Isometsä J, Jahanshah Rad Z, Fung T H, Liu H, Lehtiö J-P, Pasanen T P, Leiviskä O, Miettinen M, Laukkanen P, Kokko K, Savin H and Vähänissi V 2023 Surface passivation of Germanium with ALD Al2O3: impact of composition and crystallinity of GeOx interlayer *Crystals* **13** 667

[31] Ponath P, Posadas A B and Demkov A A 2017 Ge(001) surface cleaning methods for device integration *Appl. Phys. Rev.* **4** 021308

[32] Kumaravelu G, Alkaisi M M, Bittar A, Macdonald D and Zhao J 2004 Damage studies in dry etched textured silicon surfaces *Curr. Appl. Phys.* **4** 108–10

[33] Kim M Joong, Min K H, Park S, Song H Eun, Lee J I, Jeong K T, Park J Seong and Kang M G 2020 Study on efficiency improvement of multi-crystalline silicon solar cell by removing by-product and plasma induced damage generated during reactive ion etching *Curr. Appl. Phys.* **20** 519–24

[34] Kang D, Park H J, Choi D, Han H, Seol J, Kang Y, Lee H S and Kim D 2022 Damage and residual layer analysis of reactive ion etching textured multi-crystalline silicon wafer for application to solar cells *Sol. Energy* **233** 111–7

[35] Shim K H, Kil Y H, Yang H D, Park B K, Yang J H, Kang S, Jeong T S and Kim T S 2012 Characteristics of germanium dry etching using inductively coupled SF 6 plasma *Mater. Sci. Semicond. Process.* **15** 364–70

[36] Garin M, Heinonen J, Werner L, Pasanen T P, Vähänissi V, Haarahiltunen A, Juntunen M A and Savin H 2020 Black-silicon ultraviolet photodiodes achieve external quantum efficiency above 130% *Phys. Rev. Lett.* **125** 117702

[37] Loscutoff P W and Bent S F 2006 Reactivity of the germanium surface: Chemical passivation and functionalization *Annu. Rev. Phys. Chem.* **57** 467–95

[38] Campbell P and Green M A 1987 Light trapping properties of pyramidally textured surfaces *J. Appl. Phys.* **62** 243–9

[39] Shin S H, Liao Y, Son B, Zhao Z J, Jeong J H, Tan C S and Kim M 2021 A highly ordered and damage-free Ge inverted pyramid array structure for broadband antireflection in the mid-infrared *J. Mater. Chem.* C **9** 9884–91

[40] Staudinger P, Sistani M, Greil J, Bertagnolli E and Lugstein A 2018 Ultrascaled Germanium nanowires for highly sensitive photodetection at the quantum ballistic limit *Nano Lett.* **18** 5030–5

[41] Sistani M, Böckle R, Bartmann M G, Lugstein A and Weber W M 2021 Bias-switchable photoconductance in a nanoscale Ge photodetector operated in the negative differential resistance regime *ACS Photonics* **8** 3469–75

[42] Fang H and Hu W 2017 Photogating in low dimensional photodetectors *Adv. Sci.* **4** 1700323

[43] Kim C J, Lee H S, Cho Y J, Kang K and Jo M H 2010 Diameter-dependent internal gain in ohmic Ge nanowire photodetectors *Nano Lett.* **10** 2043–8

[44] Nagashima T, Hokoi K, Okumura K and Yamaguchi M 2006 Surface passivation for germanium and silicon back contact type photovoltaic cells *Conf. Rec. 2006 IEEE 4th World Conf. Photovolt. Energy Conversion, WCPEC-4* **1** 655–8

[45] Fernandez J 2010 *Development of Crystalline Germanium for Thermophotovoltaics and High-Efficiency Multi-Junction Solar Cells* University of Konstanz

[46] Burger T, Sempere C, Roy-Layinde B and Lenert A 2020 Present efficiencies and future opportunities in thermophotovoltaics *Joule* **4** 1660–80

[47] Jiménez A *et al* 2022 N-type doping of SiC-passivated Ge by pulsed laser melting towards the development of interdigitated back contact thermophotovoltaic devices *Sol. Energy Mater. Sol. Cells* **235** 111463

[48] Savin H, Repo P, Von Gastrow G, Ortega P, Calle E, Garín M and Alcubilla R 2015 Black silicon solar cells with interdigitated back-contacts achieve 22.1% efficiency *Nat. Nanotechnol.* **10** 624–8

[49] Martin I, Alcaniz A, Jimenez A, Lopez G, Del Canizo C and Datas A 2020 Application of Quasi-Steady-State photoconductance technique to lifetime measurements on crystalline Germanium substrates *IEEE J. Photovoltaics* **10** 1068–75